Elastic response of [111]-tunnelling impurities

2001 J. Phys.: Condens. Matter 13 1467

(http://iopscience.iop.org/0953-8984/13/7/310)

INSTITUTE OF PHYSICS PUBLISHING JOURNAL OF PHYSICS: CONDENSED MATTER

J. Phys.: Condens. Matter **13** (2001) 1467–1483 www.iop.org/Journals/cm PII: S0953-8984(01)17119-5

Elastic response of [111]-tunnelling impurities

Peter Nalbach[1], Orestis Terzidis[1,4], Karen A Topp[2] and Alois Würger[3]

[1] Institut für Theoretische Physik, Universität Heidelberg, Philosophenweg 19, 69120 Heidelberg, Germany

[2] Laboratory of Atomic and Solid State Physics, Cornell University, Ithaca, New York 14853, USA

[3] Université Bordeaux 1, CPMOH Unité Mixte de Recherche CNRS 5798, 351 cours de la Libération, 33405 Talence, France

Received 15 September 2000, in final form 7 December 2000

Abstract

We study the dynamic response of a [111] quantum impurity, such as lithium or cyanide in alkali halides, with respect to an external field coupling to the elastic quadrupole moment. Because of the particular level structure of a eight-state system on a cubic site, the elastic response function shows a biexponential relaxation feature and a van Vleck type contribution with a resonance frequency that is twice the tunnel frequency $\Delta/\hbar$. This basically differs from the dielectric response that does not show relaxation. Moreover, we show that the elastic response of a [111]-impurity cannot be reduced to that of a two-level system. In the experimental part, we report on recent sound velocity and internal friction measurements on KCl doped with cyanide at various concentrations. At low doping (45 ppm) we find the dynamics of a single [111]-impurity, whereas at higher concentrations (4700 ppm) the elastic response indicates rather strongly correlated defects. Our theoretical model provides a good description of the temperature dependence of $\delta v/v$ and Q^{-1} at low doping, in particular the relaxation peaks, the absolute values of the amplitude and the resonant contributions. From our fits we obtain the value of the elastic deformation potential $\gamma_t = 0.192$ eV.

1. Introduction

The low-temperature properties of alkali halides may be significantly modified by the presence of substitutional impurities, such as Li, CN, or OH. Already a few ppm of these defects totally change the thermal behaviour and the elastic and dielectric response below Helium temperature.

Regarding the polar molecules CN and OH, the point symmetry of the impurity site gives rise to several equivalent orientations; corresponding off-centre positions arise for the small lithium ion. Quantum tunnelling between these states results in a ground-state splitting of about 1 Kelvin. Since the number density of such tunnelling states exceeds, even at low concentration, that of small-frequency phonon modes of the host crystal, the impurities govern

[4] Currently at SAP Labs France, 505 route des Lucioles, F-06560 Valbonne, France.

0953-8984/01/071467+17$30.00

the low-temperature properties of the material. The cubic symmetry of fcc crystals favours eight defect positions in [111]-directions (CN and Li) or six positions in [100]-directions (OH in KCl). The resulting energy spectra have been discussed in detail by Gomez *et al* [1], and agree well with the Schottky peak observed by Pohl and co-workers for various impurity systems at low doping [2].

In this paper we are concerned with the elastic susceptibiltiy of a [111]-impurity. Because of the cubic symmetry, such a tunnelling system behaves in many respects as an ensemble of three two-level systems with energy splitting Δ [2, 3]. For example, the specific heat contribution of a [111]-impurity is three times the Schottky peak of a two-state system. A similar relation holds true for the dielectric response function, since the dipolar transitions occur between adjacent levels only, as indicated by the dashed lines in the actual energy spectrum shown in figure 1. This analogy has been used to describe lithium or cyanide defects in terms of a two-state approximation [4–8].

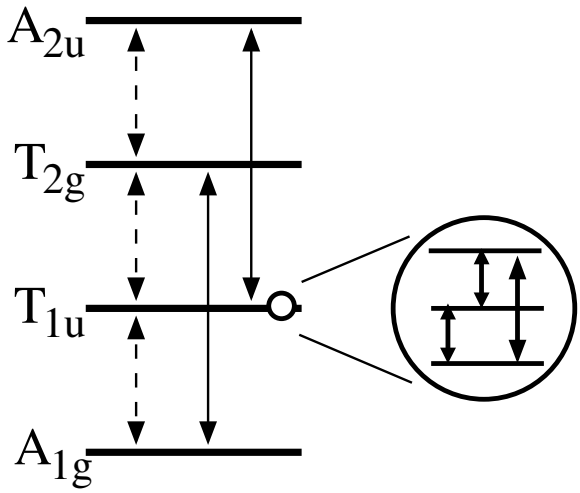

Figure 1. Energy spectrum of a [111]-impurity with zero asymmetry energy. Dashed arrows indicate the allowed dipolar transitions, and full arrows the quadrupolar ones.

The elastic response function, however, shows a more complex behaviour, resulting from the tensor character of the quadrupole operator Q_{ij} and the structure of the energy spectrum shown in figure 1. According to the allowed quadrupolar transitions indicated by solid arows in figure 1, sound waves or external stress perturb the impurity in two ways: first, they mix states separated by twice the splitting, giving rise to a van Vleck type susceptibility with resonance frequency $2\Delta/\hbar$. Second, they lift the degeneracy of the states of a given triplet level, resulting in a relaxation contribution to the response function.

Early measurements in KCl:CN samples [9] in the classical regime ($k_{\mathrm{B}}T \gg \Delta$) showed that the change of sound velocity of a T_{2g}-mode ($\hat{e} = [110]$, $\hat{k} = [001]$) varies as expected similiar to $1/T$ with temperature. Yet in addition, these experiments showed a change of sound velocity for an E_g-mode ($\hat{e} = [110]$, $\hat{k} = [1\bar{1}0]$) with an amplitude of about ten times smaller than the T_{2g} ones, whereas this mode should be unaffected according to the simplest model of a symmetric [111]-tunnelling defect.

When measuring the sound velocity (T_{2g}-mode) of KCl:Li as a function of temperature in the tunnelling regime, Hübner *et al* found a hump at $k_{\mathrm{B}}T \approx \Delta$ [10]. They related this observation to relaxational transitions between degenerate states, by calculating the static

elastic response as the second derivative of the free-energy of the impurity ion. Their results are valid in the low-frequency limit, where the external frequency is smaller than the impurity relaxation rates.

The internal friction, however, cannot be obtained from a static theory, and the low-frequency limit is not always justified for the sound velocity. Starting from standard dynamic perturbation theory, we develop a dynamic theory for the elastic response function of a [111]-impurity coupled to a phonon heat bath. The main purpose of this paper is to point out the peculiarities of the elastic response function that arise from the degenerate states of the energy spectrum shown in figure 1. Moreover, we report sound velocity and internal friction data of a T_{2g}-mode for KCl doped with cyanide molecules, and discuss them in terms of our [111]-impurity model with damping.

The outline of our paper is as follows. In section 2 we present the model and the basic equations for the elastic response function of a single impurity. The temperature dependence of the internal friction and sound velocity is evaluated in section 3. In section 4 we give some details of the experiments on KCl:CN, which are discussed in section 5. The final section contains a summary.

2. Theory

2.1. Quantum operators of a [111]-impurity

We start by discussing the properties of the energy eigenstates and by presenting our notation based on pseudospin operators. As shown in figure 1, the energy spectrum contains four equidistant levels; the upper and lower ones, A_{1g} and A_{2u}, are single quantum states, whereas the middle levels T_{1u} and T_{2g} are three-fold degenerate. This ground-state multiplet can be described as the direct product of three two-level systems with energy splitting Δ.

Each energy eigenstate is a superposition of states $|\boldsymbol{r}\rangle$ localized at the eight impurity positions

$$\boldsymbol{r} = \frac{1}{2} d(\sigma_z^1, \sigma_z^2, \sigma_z^3) \tag{1}$$

with the effective two-state coordinates σ_z^i. For a lithium impurity, the off-centre positions $\boldsymbol{r}$ form a cube of side-length d, whereas for cyanide impurities $\boldsymbol{r}$ indicates the orientation of the cigar-shaped polar molecule. Due to quantum tunnelling along the axes $i = 1, 2, 3$, the energy eigenstates factorize as $|\sigma_x^1\rangle|\sigma_x^2\rangle|\sigma_x^3\rangle$, where the variables $\sigma_x^i = \pm 1$ label odd and even superpositions $|\sigma_x^i\rangle = 2^{-1/2}\{\,|r_i = d/2\rangle + \sigma_x^i |r_i = -d/2\rangle\,\}$ along the i-axis.

Accordingly, the quantum operators of the impurity may be written as direct products of pseudospin operators σ_α^i, where $\alpha = x, y, z$ label the usual Pauli matrices and $\alpha = 0$ the identity operator. In terms of quantum states at $r_i = \pm d/2$ we have

$$\sigma_x^i = |d/2\rangle\langle -d/2| + |-d/2\rangle\langle d/2| \tag{2}$$

$$\sigma_z^i = |d/2\rangle\langle d/2| - |-d/2\rangle\langle -d/2|. \tag{3}$$

Thus a lithium or cyanide impurity is described as the product of three two-state variables. We adopt the shorthand notation for its quantum operators

$$A_{\alpha\beta\gamma} = \sigma_\alpha^1 \otimes \sigma_\beta^2 \otimes \sigma_\gamma^3 \tag{4}$$

where $i = 1, 2, 3$ label the crystal axes and Greek indices $\alpha = 0, x, y, z$ the pseudospin operators. When denoting by $\frac{1}{2}\Delta$ the tunnelling amplitude between adjacent impurity positions, we obtain the Hamiltonian

$$H_S = -\frac{\Delta}{2}\left(A_{x00} + A_{0x0} + A_{00x}\right). \tag{5}$$

Its eigenstates may be labelled according to the eigenvalues ± 1 of σ_x^i; for example, the ground-state A_{1g} reads as $|{+}{+}{+}\rangle$, and the states of the triplet level T_{1u} as $|{-}{+}{+}\rangle$, $|{+}{-}{+}\rangle$, and $|{+}{+}{-}\rangle$. According to the above discussion, the statistical operator $\rho = \mathrm{e}^{-\beta H_S}/\mathrm{tr}(\mathrm{e}^{-\beta H_S})$ factorizes as

$$\rho = \rho^1 \otimes \rho^2 \otimes \rho^3 \qquad \rho^i = \frac{1}{2}\left(1 + \sigma_x^i \tanh(\Delta/2k_\mathrm{B}T)\right). \tag{6}$$

(In the limit of zero temperature, the even-state $\sigma_x^i = 1$ is occupied with probability 1.) From the statistical operator it is evident that the specific heat anomaly due to N such defects is identical to the Schottky peak of $3N$ two-level systems with the Hamiltonian $\frac{1}{2}\Delta\sigma_x$. As to the dynamic properties, a similar relation holds true for the dielectric susceptibility. This is not surprising, since dipolar transitions involve a single coordinate r_i and occur between adjacent levels with splitting Δ only; see figure 1.

A different situation, however, is encountered when considering the elastic response: for a lattice distortion that varies sufficiently slowly in space, the interaction potential is given by the term that is linear in the elastic strain $\epsilon_{ij}(\boldsymbol{R})$,

$$W(\boldsymbol{r}) \;=\; -Q_{ij}(\boldsymbol{r})\epsilon_{ij}(\boldsymbol{r})\;. \tag{7}$$

Equation (7) is the lowest-order term of a multipole expansion with the elastic quadrupole operator

$$Q_{ij}(\boldsymbol{r}) \;=\; \sum_n R_j^n K_i^n(\boldsymbol{r}) \tag{8}$$

where $\boldsymbol{R}^n$ are the perfect lattice sites of the surrounding crystal atoms and $\boldsymbol{K}^n$ are corresponding Kanzaki forces that are related to the actual static shifts through the perfect lattice Green function [11]. For our purpose, it is sufficient to consider $\boldsymbol{K}^n$ as the force exerted by the defect at position $\boldsymbol{r}$ on the atom at site $\boldsymbol{R}^n$, in terms of the atomic potential $\boldsymbol{K}^n(\boldsymbol{r}) = -\nabla V_n(\boldsymbol{R}^n - \boldsymbol{r})$.

We recall that we are looking only for the part of $W(\boldsymbol{r})$ that depends on the defect coordinate $\boldsymbol{r}$. Thus we may expand the force $\boldsymbol{K}^n$ in terms of $\boldsymbol{r}$; due to the cubic symmetry of the crystal, the parity of the defect and the fact, that the square of the two-state coordinate $r_i^2 = d^2/4$ is a constant, the quadrupole operator reads in quadratic approximation in $\boldsymbol{r}$

$$Q_{ij} = g\, r_i r_j (1 - \delta_{ij}) \tag{9}$$

with the elastic coupling energy g. It involves two coordinates, and hence causes transitions between energy eigenstates that differ in two labels σ_x^i. Thus, elastic perturbations induce two types of transition as indicated by the solid arrows in figure 1.

2.2. *Phonon coupling*

Noting equation (1) and $A_{z00}A_{0z0} = A_{zz0}$, we may write the quadrupole operators as $Q_{12} = g(d/2)^2 A_{zz0}$, etc. With $\gamma = g(d/2)^2$, we obtain the impurity–phonon interaction [8]

$$H_{SB} = 2\sum_\alpha \gamma_\alpha \left(A_{zz0}\,\epsilon_{12}^\alpha + A_{z0z}\,\epsilon_{13}^\alpha + A_{0zz}\,\epsilon_{23}^\alpha\right). \tag{10}$$

When evaluating the strain tensor at the impurity site $\boldsymbol{R}$ and taking the limit of long wavelenths, $kd \ll 1$, we find

$$\epsilon_{ij}^\alpha = \frac{i}{2}\sum_{\boldsymbol{k}} \sqrt{\frac{\hbar}{2m\omega_{\boldsymbol{k}a}}}\,\mathrm{e}^{\mathrm{i}\boldsymbol{k}\boldsymbol{R}} \left(e_i^\alpha(\boldsymbol{k})k_j + e_j^\alpha(\boldsymbol{k})k_i\right)\left(b_{\boldsymbol{k},\alpha} + b_{-\boldsymbol{k},\alpha}^\dagger\right). \tag{11}$$

Here $\boldsymbol{k}$ and $\boldsymbol{e}^\alpha$ are wave and polarization vectors, and α labels the longitudinal and transverse phonon branches. In the following we are interested in the relaxation rates of the defect. These rates involve phonons with frequencies of about 30 GHz (corresponding to twice the energy

splitting Δ of the defect). Since the corresponding wavelength $\lambda \simeq 5\ \mu$ m (see table 1 for the speed of sound) is large compared with the size $d \simeq 1.4$ Å of the defect, the long wavelength limit is valid.

2.3. Asymmetry energy

Up to now we have considered an impurity in a potential that reflects the cubic site symmetry. The strong dipolar and elastic interactions of nearby impurities, however, break that symmetry and give rise to an effective asymmetry energy,

$$V = -\frac{v_1}{2} A_{z00} - \frac{v_2}{2} A_{0z0} - \frac{v_3}{2} A_{00z} \tag{12}$$

where the v_i are random quantities with zero mean. We assume a Gaussian distribution with width σ:

$$P(\vec{v}) = \prod_i P_i(v_i) \qquad \text{with} \qquad P_i(v_i) = \frac{1}{\sqrt{2\pi}\sigma} \exp\left(-\frac{1}{2}\frac{v_i^2}{\sigma^2}\right). \tag{13}$$

In principle, the v_i are dynamic variables closely related to the position operators of nearby impurities. In the case of weak interaction, $v_i \ll \Delta$, however, they may be treated as static random fields. Equation (12) accounts for random fields arising from dipolar interactions; elastic coupling would lead to a potential that involves quadrupole operators such as A_{zz0}.

3. Elastic response function

The lattice vibrations of the host crystal act on the tunnelling impurity as a heat bath at temperature T. Upon a perturbation by an external strain field, the impurity regains the thermal equilibrium through absorption or emission of resonant phonons. Since the impurity-phonon coupling is weak, the resulting damping rates can be evaluated in second-order perturbation theory.

3.1. Dynamic perturbation theory

The linear response of the impurity to a time-dependent external strain field is described by the commutator correlation function $\langle [Q_{ij}(t), Q_{ij}] \rangle$. For convenience, we use dimensionless quadrupole operators, e.g. $A_{zz0} = (2/d)Q_{12}$ with $\langle A_{zz0}^2 \rangle = 1$; all relevant response functions can be expressed in terms of

$$\chi(t) = \langle [A_{zz0}(t), A_{zz0}] \rangle. \tag{14}$$

It is convenient to calculate first the correlation matrix

$$C_{\alpha\beta\gamma;\delta\epsilon\zeta}(t) = (A_{\alpha\beta\gamma}(t) | A_{\delta\epsilon\zeta}) \tag{15}$$

where we have defined the symmetrized correlation function

$$(A|B) = \frac{1}{2}\langle AB + BA \rangle. \tag{16}$$

Our evaluation of the correlation matrix is based on the Mori–Zwanzig projection formalism; the resulting memory kernel is calculated to second order in the impurity-phonon coupling [12]. Thus we obtain a matrix equation for the Laplace transform of (15),

$$C(z) = \frac{-1}{z - \Omega - K(z)} M \tag{17}$$

with the usual definitions of the static correlations

$$M_{mn} = (A_m|A_n) = (\eta^{-1})_{mn} \tag{18}$$

the frequency matrix

$$\Omega_{mn} = (A_m|\mathcal{L}A_p)\eta_{pn} \tag{19}$$

and the memory kernel

$$K_{mn}(z) = (\dot{A}_m|(z-\mathcal{L}_0)^{-1}|\dot{A}_p)\eta_{pn}. \tag{20}$$

For convenience, we have replaced the triple index pair of (4) with m, n, and we have used the shorthand notations $\dot{A}_i = \mathrm{i}[H_{SB}, A_i]$ and $\hbar\mathcal{L}_0* = [H_S + H_B, *]$, where $H_B = \sum \hbar\omega_k b_k^\dagger b_k$. The thermal average $\langle \ldots \rangle$ is with respect to ρ and the equilibrium distribution of the phonons.

Solving the impurity dynamics now amounts to calculating the eigenvalues and residues of the resolvent $[z - \Omega - K]^{-1}$. Since there are 4^3 operators $A_{\alpha\beta\gamma}$, the matrix equation involves a 64-dimensional space. The matrices C, M, Ω, and K being block-diagonal, the actual problem simplifies significantly.

For symmetry reasons, the time evolution of the three operators A_{zz0}, A_{z0z}, and A_{0zz} is the same. Therefore it is sufficient to evaluate the dynamics in the invariant subspace containing one of them, e.g.

$$\begin{aligned} A_1 &= A_{zz0} \qquad A_2 = A_{zy0} \qquad A_3 = A_{yz0} \qquad A_4 = A_{yy0} \\ A_5 &= A_{zzx} \qquad A_6 = A_{zyx} \qquad A_7 = A_{yzx} \qquad A_8 = A_{yyx}. \end{aligned} \tag{21}$$

In this invariant subspace, Ω, M, and K are represented by 8×8-matrices that are easily calculated according to (18)–(20). Note that the commutation relations for the operators A_i can be traced back to those for Pauli matrices. It can be shown that Ω and M can be diagonalized simultaneously; in the present example it is straightforward to find the corresponding unitary transformation U and to obtain

$$\widetilde{\Omega} = U^\dagger \Omega U = \mathrm{diag}(0, 0, 0, 0, -2\Delta, -2\Delta, 2\Delta, 2\Delta)/\hbar \tag{22}$$

$$\widetilde{M} = U^\dagger M U = \mathrm{diag}(m_1, m_1, m_2, m_2, m_3, m_4, m_3, m_4) \tag{23}$$

with

$$\begin{aligned} m_1 &= (1-t)\,(1-t^2) \\ m_2 &= (1+t)\,(1-t^2) \\ m_3 &= (1+t)\,(1+t^2) \\ m_4 &= (1-t)\,(1+t^2) \end{aligned}$$

where we have used $\beta = 1/k_\mathrm{B}T$ and $t = \tanh(\beta\Delta/2)$.

Besides the fourfold degenerate zero frequency, there are two doubly degenerate finite frequencies $\pm 2\Delta/\hbar$ in Liouville space. While Ω and M could be diagonalized simultaneously, this is not possible for the memory matrix K. It turns out, however, that its transform $\widetilde{K}$ is diagonal in each of the three degenerate subspaces of $\widetilde{\Omega}$, with bare frequencies $0, \pm 2\Delta/\hbar$; the finite off-diagonal entries connect, e.g. the subspace of zero frequency eigenvalue with that of eigenvalue $2\Delta/\hbar$. Because of $\widetilde{K} \ll \Delta/\hbar$, we may neglect these off-diagonal entries of $\widetilde{K}$; they would result in very small corrections to the frequencies and residues of the order of $(\hbar\widetilde{K}/\Delta)^2$. In physical terms, the off-diagonal parts of $\widetilde{K}$ in the degenerate subspaces vanish, since they involve the phonon density of states at zero frequency; in a three-dimensional body, however, the density of phonon modes vanishes in the limit $\omega_k \to 0$.

Applying the usual Markov approximation, we evaluate the memory functions $\widetilde{K}(z)$ at the corresponding bare frequencies $z = 0, \pm 2\Delta/\hbar$. It is convenient to separate real and imaginary

parts according to $\widetilde{K} = \widetilde{K}' + \mathrm{i}\widetilde{K}''$. Whereas the entries in the subspace of zero eigenvalue are purely imaginary, those belonging to the finite frequencies $\pm 2\Delta/\hbar$ are complex numbers. Their real parts $\widetilde{K}'(\pm 2\Delta/\hbar)$ would induce a shift of the resonance frequencies from the bare values $\pm 2\Delta/\hbar$ to slightly smaller ones. This shift being very small, we discard it and retain the imaginary, or dissipative, part $\widetilde{K}''$ only. The latter form a diagonal matrix $\widetilde{\Gamma} = \Im\widetilde{K}''(z_0)$ with $z_0 = 0, \pm 2\Delta/\hbar$.

With these approximations for the memory kernel, $\widetilde{\Omega}$, $\widetilde{M}$, and $\widetilde{\Gamma}$ are diagonal; the correlation matrix thus factorizes,

$$\widetilde{C}_{jj}(z) = \frac{-\widetilde{M}_{jj}}{z - \widetilde{\Omega}_{jj} + \mathrm{i}\widetilde{\Gamma}_{jj}} \tag{24}$$

where $j = 1, \ldots, 8$ labels the eight eigenvalues given in equations (22) and (23) and those of the damping matrix $\widetilde{\Gamma}$. Since we are interested in the correlation function of the operator A_{zz0}, we have to calculate the element C_{11} of the correlation matrix in the original basis, $C = U\widetilde{C}U^{\dagger}$. The transformation U being unitary, we have

$$C_{11}(z) = \sum_j |U_{1j}|^2 \widetilde{C}_{jj}(z) \tag{25}$$

where the vector of coefficients

$$\left(|U_{1j}|^2\right)_j = (0, 1/4, 1/4, 0, 1/8, 1/8, 1/8, 1/8) \tag{26}$$

satisfies the condition $\sum_j |U_{1j}|^2 = 1$.

The damping rates $\widetilde{\Gamma}_{jj}$ are calculated to second-order in terms of the impurity-phonon coupling potential, equation (10). Each rate is given as the convolution of an uncoupled correlation spectrum $C^0_{ii}(\omega)$ and the dissipation spectrum, equation (A.2). The derivation is straightforward; we merely give the result

$$\widetilde{\Gamma} = \mathrm{diag}(\Gamma_1, \Gamma_1, \Gamma_2, \Gamma_2, \Gamma_3, \Gamma_4, \Gamma_3, \Gamma_4) \tag{27}$$

with

$$\begin{aligned} \Gamma_1 &= \Gamma_0(1 + n(2\Delta)) \\ \Gamma_2 &= \Gamma_0 n(2\Delta) \\ \Gamma_3 &= \Gamma_0(1 + 4n(2\Delta)) \\ \Gamma_4 &= \Gamma_0(3 + 4n(2\Delta)). \end{aligned} \tag{28}$$

Here we have used the Bose occupation factor

$$n(2\Delta) = \frac{1}{\mathrm{e}^{\beta 2\Delta} - 1} \tag{29}$$

and the coupled phonon Green function, equation (A.2) evaluated at the frequency $2\Delta/\hbar$,

$$\Gamma_0 = 2\Gamma''(2\Delta/\hbar) = \pi \sum_\alpha f_\alpha \frac{\gamma_\alpha^2}{v_\alpha^5} \frac{(2\Delta)^3}{2\pi^2\rho\hbar^4}. \tag{30}$$

The geometric factor f_α arises from the different weight for longitudinal and transverse modes in the coupling matrix elements.

Now we have an explicit expression for the frequency dependent function, equation (25). After inverse Laplace transformation we obtain the time-dependent correlation function of the operator A_{zz0},

$$C_{11}(t) = \frac{1}{4}\left(m_1\mathrm{e}^{-\Gamma_1 t} + m_2\mathrm{e}^{-\Gamma_2 t} + m_3\cos(2\Delta t + \delta_3)\mathrm{e}^{-\Gamma_3 t} + m_4\cos(2\Delta t + \delta_4)\mathrm{e}^{-\Gamma_4 t}\right) \tag{31}$$

which constitutes the basic theoretical result of this paper.

As the most salient features we note the presence of two relaxation features with different relaxation rates Γ_1 and Γ_2. The remaining terms (the so called resonant terms) show oscillations with twice the tunnelling frequency $\Delta/\hbar$ and different damping rates, with $\tan\delta_i = \hbar\Gamma_i/2\Delta$. The amplitudes m_i vary significantly with temperature; in the high-temperature limit all of them tend towards unity, $m_i \to 1$, whereas for $T \to 0$ one finds $m_3 = 4$ and $m_1 = m_2 = m_4 = 0$. Thus the relaxation contributions disappear at zero temperature.

The spectra of the response function, equation (14), and the correlation function, equation (31), are related through the fluctuation-dissipation theorem,

$$\chi''(\omega) = (2/\hbar)\tanh(\beta\hbar\omega/2)C''_{11}(\omega). \tag{32}$$

With the usual approximations for the hyperbolic tangent function we thus obtain

$$\begin{aligned}\chi''(\omega) = {} & \beta\hbar\omega\,[L_1(0) + L_2(0)] \\ & + \tanh(\beta\Delta)\,[L_3(2\Delta) - L_3(-2\Delta) + L_4(2\Delta) - L_4(-2\Delta)]\end{aligned} \tag{33}$$

with the weighted Lorentzian

$$L_i(E) = \frac{m_i}{4}\frac{\hbar\Gamma_i}{(\hbar\omega - E)^2 + \hbar^2\Gamma_i^2}. \tag{34}$$

Clearly, the spectrum of the response function $\chi''(\omega)$ contains the same physics as the correlation function C_{11}; hence the discussion below, equation (31), applies equally well to equation (33).

The tunnelling impurities can be probed by an external ultrasonic wave with propagation vector $\boldsymbol{k}$ and polarization vector $\boldsymbol{e}^\alpha$. The attenuation of the latter is given by the internal friction

$$Q_\alpha^{-1} = n\,h_{k\alpha}\frac{\gamma_\alpha^2}{\varrho v_\alpha^2}\chi''(\omega) \tag{35}$$

whereas the variation of the sound velocity

$$\frac{\delta v_\alpha}{v_\alpha} = n\,h_{k\alpha}\frac{\gamma_\alpha^2}{2\varrho v_\alpha^2}\chi'(\omega) \tag{36}$$

depends on the real part of the impurity dynamic susceptibility χ'. Here n is the number density of the impurities; the geometric factor $h_{k\alpha}$, as defined in equation (A.7), accounts for the orientation of $\boldsymbol{k}$ and $\boldsymbol{e}^\alpha$ with respect to the crystal axes.

Since the tunnelling frequency $\Delta/\hbar$ is of the order of 20 GHz, the second term of equation (33) is immaterial at acoustic frequencies; and the internal friction involves the relaxational part only,

$$Q_\alpha^{-1} = n\,h_{k\alpha}\frac{\gamma_\alpha^2}{\varrho v_\alpha^2}\frac{1}{k_\mathrm{B}T}\left[m_1\frac{\omega\Gamma_1}{\omega^2 + \Gamma_1^2} + m_2\frac{\omega\Gamma_2}{\omega^2 + \Gamma_2^2}\right]. \tag{37}$$

Note that both amplitudes are exponentially small at low temperatures, $m_1 + m_2 = 2*\mathrm{sech}(\beta\Delta/2)^2$, though m_1 vanishes faster than m_2. On the other hand, Γ_1 tends towards the constant Γ_0, whereas Γ_2 disappears. Thus, in the intermediate range $k_\mathrm{B}T \approx \Delta$ both contributions may be relevant.

Because of the different temperature dependence of the two rates and the corresponding amplitudes, the variation of Q^{-1} with frequency changes very much with the ratio ω/Γ_0. The origin of the terms in equation (37) is quite obvious in view of the level scheme of figure 1. The contribution involving Γ_2 stems from relaxation between the states of the level T_{1u}; the required intermediate transition to the top level A_{2u} accounts for the temperature factor of Γ_2. On the other hand, the term with Γ_1 results from the upper triple level T_{2g}; relaxation occurs through the intermediate state A_{1g}; phonon emission in this downscattering process gives rise

to the temperature factor of Γ_1. The rates of the resonant contributions in equation (33) can be discussed in a similar fashion.

Finally, we note that the relaxation rates Γ_1 and Γ_2 satisfy the condition $\Gamma_1 = \mathrm{e}^{\beta 2\Delta}\Gamma_2$. They are related to the phase decoherence rates Γ_3 and Γ_4 through $\Gamma_1 + \Gamma_2 = (1/4)(\Gamma_3 + \Gamma_4)$; thus the transverse rates are larger than the longitudinal ones, contrary to the well-known ratio for the two-level system, $1/T_1 = 2/T_2$.

3.2. Effects of asymmetry

In order to obtain a realistic model for tunnel impurities, we have to account for the random asymmetry fields, equation (12). At sufficiently low concentrations, $c < 100$ ppm or $n < 10^{19}$ cm^{-3}, typical values of v_i are significantly smaller than the tunnel energy Δ. Thus we may use a perturbation expansion in powers of the small parameter v_i/Δ.

Each pole of the dynamic susceptibility, equation (33), is characterized by an amplitude m_i, a damping rate Γ_i, and an oscillation frequency that takes the values $\pm 2\Delta$ or 0. It turns out that the lowest-order corrections to m_i and Γ_i are quadratic in v_i/Δ and thus are of little significance. Similarly, the finite poles at $\pm 2\Delta$ are hardly affected by the small asymmetry energies v_i.

A significant change occurs, however, in the zero-frequency poles. When evaluating equation (17) with equations (5) and (12) and calculating the lowest-order corrections in the diagonal representation, equation (24), we obtain the set of frequencies

$$\widetilde{\Omega} \approx \mathrm{diag}(\eta, \eta, -\eta, -\eta, -2\Delta, -2\Delta, 2\Delta, 2\Delta) \tag{38}$$

with

$$\eta = 1/2\,(v_1^2 - v_2^2)/\Delta. \tag{39}$$

Accordingly, the relaxation contributions $L_1(0)$ and $L_2(0)$ in equation (33) have to be replaced by $\frac{1}{2}(L_i(\eta) + L_i(-\eta))$, with $i = 1, 2$.

Since experimentally frequencies are much smaller than the tunnel frequency $\Delta/\hbar$, the imaginary part of the susceptibility is determined by the low-frequency poles $\pm\eta$. When denoting the average with respect to the random fields v_i by a bar, we have

$$\overline{\chi''(\omega)} = \frac{1}{2}\beta\omega\left(\overline{L_1(\eta)} + \overline{L_1(-\eta)} + \overline{L_2(\eta)} + \overline{L_2(-\eta)}\right). \tag{40}$$

When inserting the inverse Fourier transform of the Lorentzians, the integral over v_i involves a Gaussian with complex width parameter $(1/2\sigma^2) \pm it/\hbar\Delta$. Performing the Gaussian integrals we find

$$\overline{\chi''(\omega)} = \beta\frac{\omega\Delta}{4\sigma^2}\int_0^\infty \mathrm{d}t\,\frac{\cos(\widetilde{\omega}t)}{\sqrt{1+t^2}}\left(m_1\mathrm{e}^{-\widetilde{\Gamma}_1 t} + m_2\mathrm{e}^{-\widetilde{\Gamma}_2 t}\right) \tag{41}$$

with $\widetilde{\omega} = \omega\Delta/\sigma^2$ and $\widetilde{\Gamma} = \Gamma\Delta/\sigma^2$. We recall that we have used $k_B T, \Delta \gg \hbar\omega, \hbar\Gamma$.

Now we turn to the real part that is obtained from equation (32) through the Kramers–Kronig relation. Proceeding as above we insert the inverse Fourier tranform; resorting to the usual approximations for the temperature-dependent factors and assuming $\beta\eta/2 \ll 1$, we obtain the susceptibility

$$\chi'(\omega) = \frac{m_3 + m_4}{4}\,\frac{1}{\Delta}\tanh(\beta\Delta) + \beta\sum_{i=1,2}\sum_{\pm}\frac{m_i}{4}\,\frac{\eta(\eta \pm \omega) + \Gamma_i^2}{(\eta \pm \omega)^2 + \Gamma_i^2}. \tag{42}$$

Averaging over the distribution of asymmetries yields

$$\overline{\chi'(\omega)} \approx \frac{m_3 + m_4}{4}\,\frac{1}{\Delta}\tanh(\beta\Delta) + \sum_{l=1,2}\frac{m_l}{4}\beta\left\{1 - \frac{\omega\Delta}{\sigma^2}\int_0^\infty \mathrm{d}t\,\frac{\sin(\widetilde{\omega}t)\mathrm{e}^{-\widetilde{\Gamma}_l t}}{\sqrt{1+t^2}}\right\}. \tag{43}$$

3.3. Comparison with a two-level tunnelling system

When investigating the dynamic properties of substitutional impurities, various authors have used a two-state approximation. For this reason we briefly discuss the response function of a two-level system (TLS) and compare it with the present results for the eight-state system. With the notation introduced in section 2, the Hamiltonian of a symmetric TLS reads as

$$H = \frac{1}{2}\Delta\sigma_x + \sigma_z \sum_{\alpha,i,j} \gamma_\alpha \epsilon_{ij}^{\alpha} + H_{\text{phonon}} \tag{44}$$

which is nothing but the one-dimensional version of equations (5) and (10). When evaluating the dissipative two-state dynamics one finds that there is no relaxation contribution to the response function of a TLS; its susceptibility is of purely 'resonant' character and similar to the second term of equation (33).

Thus, the two-state approximation misses the observed relaxation peak in the dynamic response. In order to mend this failure, an asymmetry energy has been added to equation (44), yielding $H = \frac{1}{2}\Delta\sigma_x + \frac{1}{2}\epsilon\sigma_z$, with a two-level splitting $E = \sqrt{\Delta^2 + \epsilon^2}$. The spectrum of the dynamic susceptibility then reads as

$$\chi''_{zz} = \frac{\Delta^2}{E^2}\tanh(\beta E/2) \sum_{\pm} \frac{\pm\Gamma}{(\omega \mp E/\hbar)^2 + \Gamma^2} + \frac{\epsilon^2}{E^2}\operatorname{sech}^2(\beta E/2)\frac{\beta\hbar\omega \cdot (2\Gamma)}{\omega^2 + (2\Gamma)^2}. \tag{45}$$

The amplitude of the relaxation feature is proportional to ϵ^2/E^2 and thus vanishes in the limit of zero asymmetry energy. This feature distinguishes the actual eight-state system from the two-state approximation. The former contains a strong relaxation feature, even at zero asymmetry energy. The two-state approximation, however, fails to account for relaxation in the symmetric case $\epsilon = 0$.

4. Experimental detail and results

The crystals measured here were seed pulled from the melt at the crystal growth facility of the Cornell Center for Materials Research. The starting powder of KCl was Merck Industries 'Superpure' grade with nominal impurity levels of less than 1 ppm. (A check of the OH^- level in our crystal of 'pure' KCl, via UV absorption, confirmed a concentration of 0.5 ppm.) The cyanide added to the melt was taken from a seed-pulled single crystal of KCN for which the starting powder had been vacuum baked to remove H_2O.

The composition of the final crystal was analysed via infra-red absorption ($\sim 2100\ \text{cm}^{-1}$) to an estimated accuracy of 10% relative error, by comparing the area of the absorbance peak to a standard measured for us by Fritz Lüty at the University of Utah where he measured the CN^- vibrational spectra at liquid nitrogen temperature and calculated the concentration based on the known oscillator strength of CN^- [14].

The internal friction sample was cleaved directly from the IR absorption sample to ensure a known CN^- concentration. The internal friction was measured with a composite torsional oscillator as described in [15]. In this method, a 90 kHz quartz transducer (2.5 mm diameter) and the sample form a composite torsion bar. The quartz end is attached to a thin Be–Cu pedestal [15] by an approximately 25 mg drop of Stycast 2850FT epoxy, and since the KCl crystals are quite fragile, a 0.25 mm indium foil was epoxied between the crystal and transducer to 'cushion' the difference in thermal contraction rates of the two components upon being cooled. The sample length is tuned to be one half of a shear wavelength, so that the composite oscillator has a resonance frequency at room temperature within 1% of the bare quartz crystal resonance. This adjustment ensures that the epoxy and indium joint between the quartz and

sample has almost zero strain, and therefore contributes minimally to the observed internal friction. (The epoxy and epoxy/indium junctions produce a background contribution to the internal friction of less than 10^{-5} at low temperatures.)

The oscillator is driven by a set of electrodes which form a quadrupole configuration around the transducer and which simultaneously drive and detect its motion. The internal friction of the sample Q_{sa}^{-1} is determined from the quality factor Q_{comp} of the composite oscillator resonance by

$$Q_{sa}^{-1} = \left[\frac{I_{sa} + (1+\alpha)I_{tr}}{I_{sa}}\right] Q_{comp}^{-1} \tag{46}$$

where I_{tr} and I_{sa} are the moments-of-inertia of the transducer and sample respectively, and α is a correction for the attachment of the transducer to the thin Be-Cu pedestal, $\alpha \approx 0.06$ [15]. The relative change in speed of sound can be found from the change in resonance frequency of the composite oscillator

$$\frac{\Delta v}{v}_{sa} = \left[\frac{I_{sa} + (1+\alpha)I_{tr}}{I_{sa}}\right] \frac{\Delta f}{f} \tag{47}$$

where $\Delta f/f$ is determined relative to an arbitrary reference frequency usually at the coldest temperature of the run. Details on evaluating internal friction from a torsional oscillator can be found in [16]. The measurements below 1.5 K were made in a dilution refrigerator, and those from 1.5 to 300 K in an insertable ^{4}He cryostat [17].

We have investigated a T_{2g}-mode ($\hat{e} = [110]$, $\hat{k} = [001]$) in three samples doped with 45, 370 and 4700 ppm CN^-, and a pure sample; the latter provides the background due to the host crystal and thus permits us to determine the impurity contribution to the elastic response function.

Figure 2 shows the internal friction as a function of temperature, cyanide concentration ranging from 0 to 4700 ppm. The data consist of several peaks. The dominant feature occurs at about 450 mK in the 45 ppm data and moves to about 350 mK in the 370 ppm-data; in the strongly doped sample (4700 ppm) it results in a broad shoulder beyond the lowest temperatures investigated. At higher T there are additional peaks with a much weaker intensity, which may well result from strongly coupled defect pairs [19]. The internal friction of the undoped sample is significantly smaller, although still remarkably high. (Even after a check for purity, there is still some unexpected damping in the 'pure' KCl. The expected background internal friction value for pure crystals using this technique is less than 3×10^{-6} below 1 K, as measured in quartz [16].)

The relative change of the sound velocity is plotted in figure 3. The temperature dependence of the data may be decomposed into two features. First, there is a contribution proportional to $\tanh(E/2kT)$ with an energy E of a few K, that is characteristic for quantum defects and shows the well known $1/T$-dependence at higher temperature. Second, the minimum at $T = 0.7$ K indicates a relaxation process.

Though the minimum broadens with increasing doping, the three samples show quite a similar behaviour, and the change in sound velocity is roughly linear in the impurity concentration.

5. Comparison of theory and experiment

We focus on the data of KCL with 45 ppm CN^- since our theory is correct for low doping only, i.e. for impurities without interaction. With increasing doping, however, their dipolar interactions are no longer small. The collective dynamics result in the broad internal friction

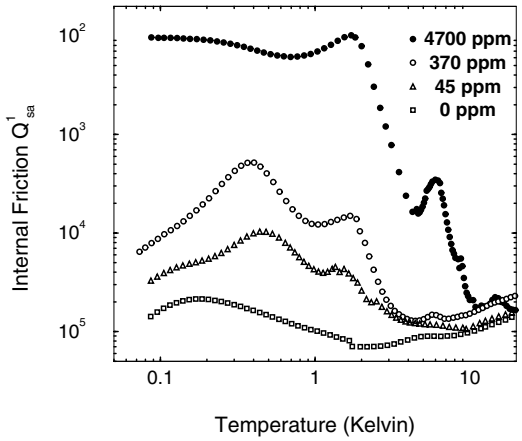

Figure 2. The internal friction data of four KCl samples with different concentrations of CN^- dopants are plotted versus the temperature.

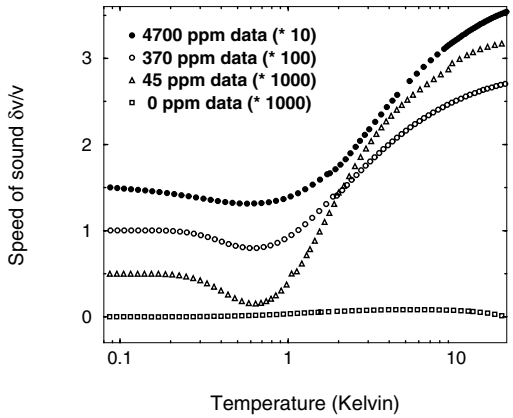

Figure 3. Relative change of sound velocity $\delta v/v$ for four KCl samples with different concentrations of CN^- dopants are plotted versus the temperature. For convenience, the data are multiplied by the factors of 10. Note the vertical shift by steps of 0.5 with respect to the somewhat arbitrary origin at zero temperature.

spectrum shown in figure 2 at higher concentrations; the sharp features indicate strongly coupled impurity pairs.

The theoretical expressions for symmetric tunnel impurities involve the tunnel energy Δ and the damping rate Γ_0, equation (30); taking also finite asymmetry energies as in section 2.3 into account, the Gaussian width σ provides one more parameter. Both the rate Γ_0 and the prefactors of the internal friction and the change of sound velocity (equations (35) and (36)) depend on the deformation potentials γ_α, the sound velocities v_α and the mass density of the host crystal ϱ. The latter quantities are well known; since the longitudinal sound velocity is significantly larger than the transverse one, we have $v_t^{-5} \gg v_l^{-5}$ and retain transverse sound waves only, with $v_t = 1.7$ km s^{-1} and $\varrho = 1.989$ g cm^{-3}. (We neglect the weak dependence of the sound velocity on the propagation direction.)

The tunnel energy Δ/k_B of CN in KCl has been measured by various techniques, with different experimental results, such as; paraelectric resonance: 1.87 K [23]; excitation of

optical vibrations: 1.73 K [24]; specific heat: 1.6 K [25]. The relatively large discrepancy between these values may be due to experimental uncertainties and different parameters of the samples, in particular impurity concentration. From our fits to the 45 ppm data we obtained a value of 1.55 K, which is in reasonable agreement with the above results. Regarding the asymmetry energy, we use $\sigma/k_B = 0.0145$ K for the width of the Gaussian distribution. Finally, the transverse deformation potential γ_t constitutes the most important parameter, appearing both in the prefactors and relaxation rates. From our fits we obtain the value $\gamma_t = 0.192$ eV which is of the same order of magnitude as the values obtained for OH impurities in KCl (1 eV) [26], in NaCl (1.0 eV) [27] and OD in NaCl (0.34 eV) [27].

First we discuss the internal friction as shown in figure 4. The triangles are the background corrected data of the 45 ppm sample, i.e. we have subtracted from the original data the values for the undoped sample. The full line is a fit including asymmetry effects (41) where we used the parameters given in table 1.

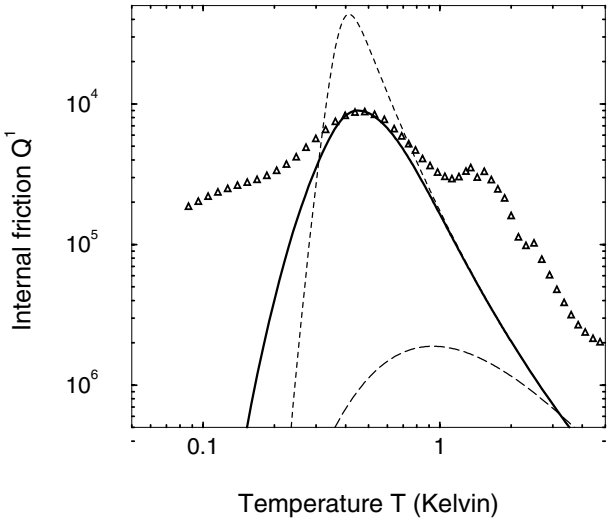

Figure 4. The [111]-defect theory is fitted at the data of the internal friction of the KCl: 45 ppm CN^- sample. The full line is a fit including asymmetry effects and the short-dashed line without these. The long-dashed line shows a plot of the internal friction of a two-level-system where we set $(\epsilon/E) = 1$ whereas all other parameters was chosen the same as in the former fit.

Table 1. Parameters used for the fits of figures 4 and 5.

$\omega/2\pi$ (sec^{-1})	n (cm^{-3})	ϱ (g cm^{-3})	v_t (km s^{-1})	Δ/k_B (K)	γ_t (eV)	σ/k_B (K)
84352	1.7×10^{17}	1.989	1.7	1.55	0.192	0.0145

The temperature where the maximum occurs depends strongly on the tunnelling amplitude Δ and the fraction ω/Γ_0; the maximum value of Q^{-1} varies with the prefactor and the asymmetry width as far as the mean splitting is bigger than the frequency $\bar{\eta} = \sigma^2/\Delta \geqslant \omega$.

The relaxation peak arises where the external frequency is comparable to the slow rate Γ_2, and $T_{\max}$ is determined by the relation $\Gamma_2(T_{\max}) = \omega$. Thus the exponential decrease of Γ_2 is essential for the existence of the relaxation maximum.

Note that this mechanism does not exist for two-level tunnelling systems, even with large asymmetries, since their relaxation rate tends towards a constant Γ_0. As a consequence,

for $\omega \ll \Gamma_0$ the relaxation maximum is suppressed by a factor ω/Γ_0, and the internal friction of a two-level system is by two orders of magnitude smaller than that obtained for the [111]-impurity model. Note that the parameters gathered in table 1 result in a rate constant $\Gamma_0 = 1.35 \times 10^9\ \mathrm{sec}^{-1}$ which is indeed much larger than the frequency $\omega = 5.3 \times 10^5\ \mathrm{sec}^{-1}$. For systems with $\eta > \omega$ the peak is suppressed by ω/η (see equation (40)) which means that the peak contribution stems from systems with small asymmetries. Therefore, the peak in the internal friction data determines only a combination of the prefactor and the asymmetry width.

Our simple model accounts well for the position and height of the peak and for its shape close to the maximum. Yet it strongly underestimates the wings at temperatures well above and below $T_{\max}$. As to the excess spectral weight observed at low temperatures, a more realistic distribution of asymmetry energies would probably give a better agreement than the Gaussian used in equation (41). The additional peak at about 2 K may well be due to strongly coupled pairs.

Now we turn to the relative change of sound velocity as shown in figure 5. The triangles are data for the 45 ppm sample. The dashed line is a fit without asymmetry, given by equation (36), and the full line with asymmetry, equation (43). The asymmetry distribution with width σ merely smears out the temperature dependence. Thus, the fit of figure 5 mainly depends on the tunnelling amplitude and the prefactor but it hardly varies with the relaxation rate and the asymmetry width.

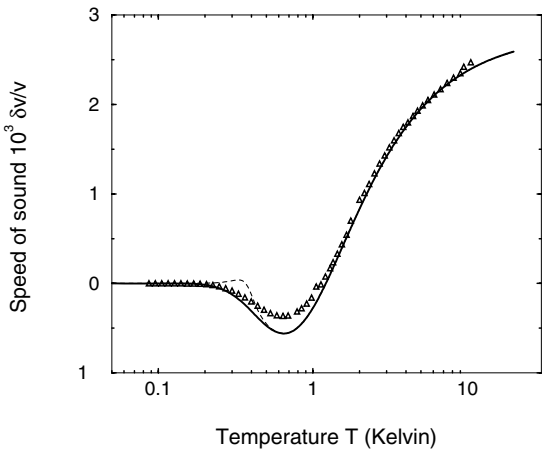

Figure 5. The [111]-defect theory is fitted at the data of the relative change in speed of sound of the KCl: 45 ppm CN^- sample. The full line is a fit including asymmetry effects and the dashed line without.

Regarding figures 4 and 5, our model fits remarkably well the absolute values of $\delta v/v$ and Q^{-1}, the hump in the sound velocity, and the position of the relaxation peak in the internal friction. The transverse deformation potential is the most relevant parameter that determines both the absolute values of $\delta v/v$ and Q^{-1}, and the relaxation maximum of the latter; we find the value $\gamma_t = 0.192$ eV. (Note the factor 2 in our definition of the phonon coupling, equation (10).)

The width of the relaxation peak of Q^{-1} and the low-temperature wing indicate the relevance of the asymmetry energies, equation (12). The poor quality of our fit at low T may well be due to the choice of a Gaussian distribution for the asymmetries. Nonetheless, our results confirm that for the 45 ppm sample, the mean asymmetry is by two orders of magnitude smaller than the tunnel energy, which is consistent with the model assumptions.

The present theory accounts fairly well for available data on the relaxation behaviour of [111]-impurities in alkali halides investigated with T_{2g}-modes, in particular with respect to the temperature dependence. Yet the multiexponential decay with the two rates Γ_1 and Γ_2 gives rise to quite an intricate relaxation spectrum; thus an experimental investigation of the frequency dependence would seem most promising. Simliar behaviour was also found for an E_g-mode [9] contradicting the simplest model of an [111]-defect. Even asymmetries cannot explain this feature in a simple way. Another open question concerns the thermal conductivity [2]. The relaxation feature obtained in the present work should significantly contribute to thermal resistivity at low T. Still, the spectrum of the defects obtained from the data [2] suggests a more complicated elastic response spectrum and may well require large asymmetry energies.

Another interesting point would be to extend the present work to the case of strong doping; this is certainly not an easy task, given the serious difficulties encountered already in the treatment of interacting two-state systems (see, e.g. [28].) Note, however, that our sound velocity data in figure 3 depend, roughly speaking, linearly on the impurity concentration. Thus, it would seem that they do not fullfil the strong-coupling criterion of [8], i.e.
the dipolar interactions have not yet destroyed the coherent tunnel motion.

6. Summary

We have investigated the relaxation of an impurity ion in alkali halides arising from the coupling to elastic waves. We briefly summarize the main results.

(i) The various elastic and inelastic phonon-mediated transition between the eight quantum states give rise to an intricate temperature and frequency dependence of the relaxation contributions to the internal friction and the sound velocity (see figure 1). Unlike two-state tunnelling systems, [111]-impurities show two relaxation rates. At low T, the smaller rate decreases exponentially, $\Gamma_2 = \mathrm{e}^{-2\Delta/kT}\Gamma_0$, whereas the larger one tends towards a constant, $\Gamma_1 = \Gamma_0$. This corresponds to a multiexponential decay of the time-dependent response and correlation functions (equations (14) and (31)).

(ii) A most particular relaxation behaviour arises for external frequencies ω that are smaller than the constant rate, $\omega < \Gamma_0$. Then the relaxation maximum occurs at a temperature where the smaller rate Γ_2 is equal to the external frequency ω. This maximum is the more relevant as at low T the spectral weight of the slow contribution exceeds by far that of the faster rate Γ_1.

(iii) Comparison with recent data on KCl:CN proves the relevance of this relaxation mechanism. The exponentially decreasing rate Γ_2 explains the large amplitude of the relaxation peak shown by the external friction Q^{-1} as a function of temperature at $\nu = 84$ kHz. By the same token, our model provides a good description for the hump in the sound velocity.

(iv) The prefactors of $\delta v/v$ and Q^{-1} and the relaxation rates are related by the values for the deformation potential γ, sound velocity v, and mass density ρ. By taking γ as a free parameter, we obtain reasonable values of γ (compared with similiar materials) satisfying fits for $\delta v/v$ and Q^{-1}, involving both absolute values and the temperature dependencies.

(v) The phenomena mentioned in (iii) cannot be explained in terms of relaxation of corresponding two-level systems. For the latter, the low-temperature rate tends towards a constant and thus may exceed ω at any T, whereas the small rate Γ_2 of a [111]-impurity inevitably meets ω at some T and gives rise to a relaxation peak. Though certain aspects of the thermal and dielectric properties of such doped crystals are described by a ensemble

of two-state systems, such a model fails in view of the acoustic properties, due to the multiexponential decay of the elastic response function, equation (14).

Acknowledgment

We would like to express a special thankyou to Professor Robert Pohl for his guidance on the experiments as well as many stimulating discussions and helpful comments on this manuscript. We also wish to thank C Enss for stimulating the theoretical investigation and H Horner, R Kühn and B Thimmel for many helpful discussions. Additionaly P Nalbach wants to thank the DFG which supported the work within the DFG-project HO 766/5-3 'Wechselwirkende Tunnelsysteme in Gläsern und Kristallen bei tiefen Temperaturen'.

Appendix A. Geometric factor of the [111]-impurity

Time evolution of the phonon heat bath is given by the lattice response function ($t \geqslant 0$)

$$\Gamma(t) = \sum_{\alpha} \frac{\gamma_\alpha^2}{\hbar^2} \overline{\langle [\epsilon_{ij}^\alpha(t), \epsilon_{ij}^\alpha] \rangle} \tag{A.1}$$

where $i \neq j$ and the bar indicates the average over crystal axes. The entries of the damping matrix, equation (20), are determined by the coupled phonon spectrum; in the limit of long wavelengths one has

$$\Gamma''(\omega) = \frac{\pi}{2} \sum_{k\alpha} f_{k\alpha}^{(ij)} \gamma_\alpha^2 \frac{k^2}{m\hbar\omega_{k\alpha}} [\delta(\omega - \omega_{k\alpha}) - \delta(\omega + \omega_{k\alpha})] \tag{A.2}$$

where

$$f_{k\alpha}^{(ij)} = \left(e_i^\alpha(\boldsymbol{k}) \hat{k}_j + e_j^\alpha(\boldsymbol{k}) \hat{k}_i \right)^2 \tag{A.3}$$

accounts for the orientations of wave and polarizations vectors with respect to the crystal axes. For an isotropic phonon density of states, the sum over phonon modes becomes

$$\frac{1}{V} \sum_{k,\alpha} f_{k\alpha}^{(ij)}(\ldots) \longrightarrow \frac{1}{2\pi^2} \sum_{\alpha} f_\alpha \int_0^K \mathrm{d}k k^2 (\ldots) \tag{A.4}$$

where we have for each polarization defined the average value

$$f_\alpha = \frac{1}{4\pi} \int \mathrm{d}\Omega f_{k\alpha}^{(ij)}. \tag{A.5}$$

In the Debye model with $\omega_{k\alpha} = v_\alpha k$, the damping spectrum finally reads as

$$\Gamma''(\omega) = \frac{\pi}{2} \sum_{k\alpha} f_\alpha \frac{\gamma_\alpha^2}{v_\alpha^5} \frac{\omega^3}{2\pi^2 \rho\hbar}. \tag{A.6}$$

Since an elastic wave couples via each of the quadrupole operators to the defect according to equation (10), the geometric factor $h_{k\alpha}$ of the internal friction and the relative change of the sound velocity of an elastic wave with propagation vector $\boldsymbol{k}$ and polarization vector $\boldsymbol{e}^\alpha$ gets

$$h_{k\alpha} = f_{k\alpha}^{(12)} + f_{k\alpha}^{(13)} + f_{k\alpha}^{(23)}. \tag{A.7}$$

The factors f_α are easily evaluated after expressing the unit vectors $\hat{\boldsymbol{k}} = \boldsymbol{k}/k$ and $\boldsymbol{e}$ in polar coordinates θ and ϕ. Putting $\hat{\boldsymbol{k}} = (\sin\theta\sin\phi, \sin\theta\cos\phi, \cos\theta)$, one finds for the longitudinal case $\boldsymbol{e}^1 = \hat{\boldsymbol{k}}$ the factor $f_l = 4/15$.

Regarding the transverse modes, we obtain $f_{t_2} = 8/45$ for $e^2 = (\cos\phi, -\sin\phi, 0)$ and $f_{t_3} = 2/9$ for the remaining polarization e^3. Though these values depend on the choice of e^2 and e^3, their average $f_t = (1/2)(f_{t_2} + f_{t_3}) = 1/5$ is independent of the basis. Defining moreover the mean value of the three polarization directions, $f = (1/3)(f_l + 2f_t)$, we finally have

$$f_l = \frac{4}{15} \qquad f_t = \frac{1}{5} \qquad f = \frac{2}{9}. \tag{A.8}$$

Thus the quantity, equation (A.3), for longitudinal modes is by a factor $f_l/f_t = 4/3$ larger than the transverse ones. In the average, propagation and polarization directions are uncorrelated, resulting in

$$f = \left(\langle \hat{k}_i^2 \rangle \langle e_j^2 \rangle + \langle \hat{k}_j^2 \rangle \langle e_i^2 \rangle\right) = 2(1/3)^2. \tag{A.9}$$

References

[1] Gomez M, Bowen S P, Krumhansl J A 1967 *Phys. Rev.* B **153** 1009
[2] Narayanamurti V and Pohl R O 1970 *Rev. Mod. Phys.* **42** 201
[3] Nalbach P and Terzidis O 1997 *J. Phys.: Condens. Matter* **9** 8561
[4] Baur M E and Salzman W R 1969 *Phys. Rev.* **178** 1440
[5] Klein M W 1984 *Phys. Rev.* B **29** 5825
Klein M W 1985 *Phys. Rev.* B **31** 2528
[6] Kranjc T 1992 *J. Phys. A: Math. Gen.* **25** 3065
[7] Terzidis O and Würger A 1996 *J. Phys.: Condens. Matter.* **8** 7303
Terzidis O 1995 Thesis Ruprecht-Karls-Universität Heidelberg
[8] Würger A 1997 *From Coherent Tunnelling to Relaxation, Springer Tracts in Modern Phys.* vol 135 (Berlin *et al*: Springer)
[9] Byer N E and Sack H S 1968 *Phys. Stat. Sol.* **30** 569
[10] Hübner M 1994 Thesis Ruprecht-Karls-Universität Heidelberg
[11] Leibfried G and Breuer N 1978 *Point Defects in Metals, Springer Tracts in Modern Phys.* vol 81 (Berlin *et al*: Springer)
[12] Mori H 1965 *Prog. Theor. Phys.* **33** 127
Zwanzig R 1960 *J. Chem. Phys.* **33** 1338
[13] Topp K A 1997 Thesis Cornell University
[14] Lüty F 1974 *Phys. Rev.* B **10** 3677
[15] Cahill D G and Van Cleve J E 1989 *Rev. Sci. Instrum.* **60** 2706
[16] Topp K A, Thompson E and Pohl R O 1999 *Phys. Rev.* B **60** 898
[17] Swartz E T 1986 *Rev. Sci. Instrum.* **57** 2848
[18] Classen J, Enss C, Bechinger C, Weiss G and Hunklinger S 1994 *Ann. Physik* **3** 315
[19] Enss C 1996 private communication
[20] Jäckle J 1972 *Z. Phys.* **257** 212
[21] Hunklinger S and Raychaudhuri A K 1986 *Prog. in Low-Temperature Physics* ed D F Brewer (Amsterdam: Elsevier)
[22] Würger A 1998 *Tunneling Systems in Amorphous and Cristalline Solids* ed P Esquinazi (Berlin *et al*: Springer)
[23] Holuj F and Bridges F 1979 *Phys. Rev.* B **20** 3578
[24] Lüty F 1974 *Phys. Rev.* B **10** 3677
[25] Peressini P P, Harrison J P and Pohl R O 1969 *Phys. Rev.* **182** 939
[26] Roberts S 1951 *Phys. Rev.* **81** 865
[27] Burst M 1999 Thesis Universität Karlsruhe
[28] Kühn R and Würger A 2000 *Phys. Rev.* B **62** 12 069